The linewidth enhancement factor of intersubband lasers: from a two-level limit to gain without inversion conditions

FERNANDES PEREIRA, Mauro <http://orcid.org/0000-0002-2276-2095>

Editorially accepted for publication at Applied Physics Letters on 15-11-2016

The Linewidth Enhancement Factor of Intersubband Lasers: From a Two-Level Limit to Gain without Inversion Conditions

M.F. Pereira[a)]

Materials and Engineering Research Institute, Sheffield Hallam University, S1 1WB, Sheffield, UK

The linewidth enhancement (α factor) due to fluctuations in the refractive index induced by carrier fluctuations of intersubband lasers was initially expected to be zero. However, values ranging from -0.5 to 3 have been found experimentally. This paper resolves this controversy showing that counter rotating terms, usually ignored in simulations are the actual fundamental origin of nonzero α at peak gain even without inclusion of nonparabolicity and manybody effects, which are however needed to explain negative values. For laser without inversion conditions, significant as a potential out of the box solution for the elusive room temperature operation of terahertz lasers, α is found to be larger, but still at the same order of magnitude of conventional inverted medium lasers, thus ensuring their applicability to a huge number of spectroscopic applications which require sharp laser linewidths.

Understanding and controlling the linewidth of an intersubband laser is crucial from a fundamental quantum optical point and all the more so for a wide range of spectroscopic applications, since all gases and bio-materials of increasingly interest for both basic science and applications have strong absorption signatures in the Mid Infrared or THz. Intersubband lasers, such as Quantum Cascade Lasers (QCLs), are the prime sources for this range and in order to use them to detect and distinguish different gases with high sensitivity a narrow laser linewidth is required [1]. The linewidth of a conventional laser stems from fluctuations in the laser field due to spontaneous emission, described by the Schawlow-Townes formula [2], $\Delta\nu_{ST} = A/n_{ss}$, where A is the spontaneous emission coefficient and n_{ss} is the number of photons in the lasing mode at steady state. In addition to that, in a semiconductor laser there is a contribution arising from fluctuations in the refractive index induced by carrier density fluctuations. The later are quantitatively characterized by the linewidth enhancement or α factor $\Delta\nu = (1+\alpha^2)\,\Delta\nu_{ST}$ [3].

In QCLs, the usual well and barrier materials (such as GaAs and $Ga_{1-x}Al_xAs$) used to create the structure lead to lasing transitions between subbands with almost identical effective masses. As a consequence,

a) Electronic mail: m.pereira@shu.ac.uk

the gain remains quasi-symmetrical and the α factor was originally expected to be close to zero, but in contrast, a relatively large spread of values has been found experimentally: sub-threshold linewidth enhancement factor was measured with values ranging from -0.5 to 0.5 [4] and the above-threshold linewidth enhancement factor at room temperature was found between 0.2 and 3 [5,6]. For the THz case α between 0.2 and 0.5 has been reported [7].

The THz case is challenging, because the scattering and dephasing mechanisms can have the same order of magnitude as a THz lasing transition making it impossible to reach population inversion at room or close to room temperatures and the record of 200 K operation has not improved since 2012 [8]. Hence the relevance of gain without inversion (GWI) as a possible out of box solution for the problem and crucially for the context of this study, nonequilibrium GWI has a dispersive lineshape, in contrast with the usual Lorentzian-like spectrum of a fully inverted intersubband gain medium [9].

Nonparabolicity in the bandstructure and manybody effects are taken into account here with a Nonequilibrium Green's Functions approach [10, 11]. These effects have been recently attributed as being the origin of a nonzero α factor at peak intersubband gain [12]. However this paper shows that a nonzero value is to be expected due a simpler and more fundamental reason, namely one should not make the rotating wave approximation when calculating interesubband α. Furthermore, it predicts what happens when the intersubband gain lineshape deviates strongly from the ideal Lorentzian case, specifically when it is dispersive under GWI conditions.

Finally, a system where the evolution of the gain lineshape from Lorentzian-like with population inversion and dispersive-like under GWI conditions can be controlled is required. The ideal candidate is thus a dilute nitride quantum well, where the addition of a small concentration of Nitrogen in GaAs quantum wells, allows the bandstructure to be engineered delivering a dispersive gain shape with efficient intersubband GWI. Under conventional inverted band conditions, Lorentzian gain is obtained, so the total number of electrons in each subband must be controlled. This can be obtained in practice by optical pumping, selective doping or a combination of both methods.

This paper starts with a general, system-independent discussion and analytical limits delivering global conclusions, which are followed by full numerical results for dilute nitrides and a brief summary.

Independently of the material system under consideration, the α factor, α (E) and gain g(E) spectra as a function of photon energy E are obtained from the optical susceptibility χ(E) [11]. CGS units are used throughout the text.

$$\alpha(E) = \frac{\delta Re\{\chi(E)\}}{\delta Im\{\chi(E)\}}, \quad g(E) = -\frac{4\pi E}{c\hbar n_b} Im\{\chi(E)\}. \tag{1}$$

Here n_b denotes the background refractive index and c is the speed of light. The optical susceptibility is derived in linear response to a probing electromagnetic field and is directly expressed as function of the carriers Green's function (GF). When interactions within the system are taken into account, the corresponding Dyson Equation can have all its terms expanded in terms of the Hamiltonian describing the underlying arbitrary material system. Representation of the Dyson Equation in a specific basis leads to an integro-differential equation for the GF and for the optical susceptibility. Considering the set of quantum numbers {μ **k**} and explicitly including the interaction of the probe electromagnetic field with matter, and after Fourier transform to frequency (or equivalently Energy) and k-space we obtain

$$\chi(E) = 2/\Omega \sum_{\mu,\nu\neq\mu,\boldsymbol{k}} \wp_{\mu\nu\boldsymbol{k}}\, \chi_{\nu\mu}(\boldsymbol{k}, E), \tag{2}$$

where $\wp_{\mu\nu k} = e\, d_{\mu\nu k}$ is the transition dipole moment between the states (or subbands, depending on the system under consideration) ν, μ, is the sample volume and e is the electron charge. Note that by summing over all possible subbands we take into account both resonant, or rotating wave approximation (RWA) and counter-rotating contributions (CRWA). The nonequilibrium population difference between states (or subbands) ν and μ is denoted $N_{\nu\mu k} = N_\nu(k) - N_\mu(k)$. The real and imaginary terms of the selfenergies characterizing the interacting system define the renormalized energies $\varepsilon_{\nu\mu k} = \varepsilon_\nu(k) - \varepsilon_\mu(k)$ and dephasing $\Gamma_{\nu\mu k}$ [10, 11]. Only electron-electron scattering is included in the numerical solutions presented in this paper. Detailed derivations connecting the Dyson equations to the susceptibility are given in Ref. [13] for interband optics and in Refs. [14, 15] for the intersubband case.

The Coulomb interaction gives rise to a coupling term $V_{kk'}^{\nu\mu}$. For generality k is written as a vector to include, e.g. the intersubband transition case where it denotes two-dimensional crystal momentum. Introducing a quasi-free carrier susceptibility matrix element $\chi_{\nu\mu}^0(\boldsymbol{k}, E)$ and the interaction matrix element $\mathcal{F}_{\boldsymbol{k}\boldsymbol{k}'}^{\nu\mu}$,

$$\chi_{\nu\mu}^0(\boldsymbol{k}, E) = \frac{\wp_{\nu\mu\boldsymbol{k}}\, N_{\nu\mu\boldsymbol{k}}}{E - \varepsilon_{\nu\mu\boldsymbol{k}} + i\Gamma_{\nu\mu\boldsymbol{k}}}, \tag{3}$$

$$\mathcal{F}_{\boldsymbol{k}\boldsymbol{k}'}^{\nu\mu} = \delta_{\boldsymbol{k}-\boldsymbol{k}'} - \frac{N_{\nu\mu\boldsymbol{k}}}{E-\varepsilon_{\nu\mu\boldsymbol{k}}+i\Gamma_{\nu\mu\boldsymbol{k}}} V_{\boldsymbol{k}\boldsymbol{k}'}^{\nu\mu}, \tag{4}$$

The equation for $\chi_{\nu\mu}(\mathrm{k},\mathrm{E})$ is obtained by multiplication by the inverse matrix $\left(\mathcal{F}_{\boldsymbol{k}\boldsymbol{k}'}^{\nu\mu}\right)^{-1}$

$$\chi_{\nu\mu}(\boldsymbol{k},E) = \sum_{\boldsymbol{k}'}\left(\mathcal{F}_{\boldsymbol{k}\boldsymbol{k}'}^{\nu\mu}\right)^{-1} \chi_{\nu\mu}^{0}(\boldsymbol{k}',E), \tag{5}$$

Which reduces to Eq. (2) of Ref. [14] if only the electron-electron interaction is considered.

Let's start by drawing system-independent conclusions. Assuming only one transition, dispersionless energy differences, as in the case of identical effective masses on both subbands for intersuuband transitions and k-independent dipole moments, $\wp_{\nu\mu\boldsymbol{k}} \equiv \wp$. Without manybody effects, the dephasing and renormalized energies become fully k-independent, $\varepsilon_{\nu\mu\boldsymbol{k}} \equiv \Delta$ and , $\Gamma_{\nu\mu\boldsymbol{k}} \equiv \Gamma$. The change in optical susceptibility due to a total change in occupation density δn (after sum over k, with a factor 2 for spin and division by the volume Ω) and the corresponding α factor read

$$\delta\chi(E) = \frac{|\wp|^2\delta n}{\Omega}\left[\frac{1}{E-\Delta+i\Gamma} - \frac{1}{E+\Delta+i\Gamma}\right], \tag{6}$$

$$\alpha(E) = \frac{\Delta^2+\Gamma^2-E^2}{2\Gamma E}. \tag{7}$$

This very simple and general expression, which has the same structure of a two-level atom, captures all qualitative features of the α factor. It diverges as 1/E for small energies, and goes from positive to negative around peak gain. Note that the CRWA term (second fraction in δχ does not affect the peak gain position which is still almost exactly at E=Δ, unless the dephasing is comparable with the transition energy. Moreover the real part change is not zero any more at E=Δ and since the α factor is the ratio of two small nonzero quantities, the CRWA terms are the thus the fundamental origin of a nonzero α factor at peak gain, $\alpha_{\mathrm{peak}} = \Gamma/2\Delta > 0$, even without nonparabolicity and manybody effects. These terms have not been considered in previous studies [12]. However, nonparabolicity or at least k-dependent bandgap shifts are indeed required to explain a negative α factor. This is of course enhanced by the full many body effects in Eq. 5. The k-dependence in $\varepsilon_{\nu\mu\boldsymbol{k}}$ allows the phase space filling in $N_{\nu\mu\boldsymbol{k}}$ to deliver a blue-shift in the peak gain, so that α at peak gain can be zero or negative. Full numerical solutions of Eq.s 1 to 5 are thus needed and are discussed next.

The structure considered for full numerical studies is the 7 nm $Ga_{0.98}N_{0.02}As$-$Al_{0.3}Ga_{0.7}As$ quantum well of Ref. [11]. The only subbands needed are denoted for simplicity e_1, e_2 and e_3. There is no need to consider other subbands because if electrons are injected in e_3, the only allowed dipole moments are given by $d_{1,3}$ = 0.216 nm, and $d_{2,3}$ = 0.313 nm. In all figures, the carrier density for the upper e_3 subband

is denoted N_{up} while the densities of the lower bands e_1 and e_2 are $N_{e1} = N_{e2} = N_{low}$. They correspond respectively to e_{1-}, e_{3-} and e_{2+} in the notation of Ref. [11]. This structure delivers significant GWI because the conduction subbands have been engineered with dilute nitride doping leading to dispersion relations with the effective masses in the upper bands lower than those below. The effective masses at k=0 are given by m_1=0.125, m_2=0.820 and m_3=0.109, in good agreement with experiments [16].
These subbands are farther apart energetically than the first two quantum well subbands usually investigated in intersubband optics. This is why the energies that appear in the numerical results are of the order of 800 meV and not the usual values around 100 meV seen typically in the literature.

The numerical scheme can be summarised as follows: The first step is the solution of the 10 band $\boldsymbol{k \cdot p}$ Hamiltonian which includes the dilute nitrogen levels responsible for the extra nonparabolicity that controls the resulting effective subband masses and ultimately lead to engineering the occupation functions for local gain in k-space without global population inversion [11]. The Green's functions and selfenergies are expanded using eigenstates and eigenvalues of this Hamiltonian. The system is globally out of equilibrium but the electrons are assumed to be independently thermalised within each subband at 300 K with occupation functions characterised by temperatures which can be extremely different from the lattice temperature, similarly to the case of electrons in conduction-band based QCLs as found in micro-probe photoluminescence experiments [17].
Matrix numerical inversion of the integro-differential Eq. 5 allows the calculation of the curves shown next after substitution of $\chi_{\nu\mu}(\boldsymbol{k}, E)$ into Eq. 2. The integro-differential equation for the susceptibility is solved numerically in this paper including manybody effects, nonparabolic bandstructure, correlation, and dephasing mechanisms, for the case of electron-electron scattering. Expressions for the broadening, selfenergies and the Coulomb matrix elements $V_{\boldsymbol{kk'}}^{\nu\mu}$ are given in Refs. [14, 15].
Figure 1 illustrates the evolution of the α factor spectrum from GWI dispersive gain conditions to extremely inverted double Lorentzian gain with subband occupations given by N_{low},N_{up} = (1,1), (1,4) and (1,30) $\times 10^{11}$ cm^{-2}, respectively for the solid-black, dashed-blue and dot-dashed-red curves. The insets show real and imaginary parts of the susceptibility for the first two cases with matching colour and curve codes. The low and high energy peaks correspond respectively to the e_3 to e_2 and e_3 to e_1 transitions.

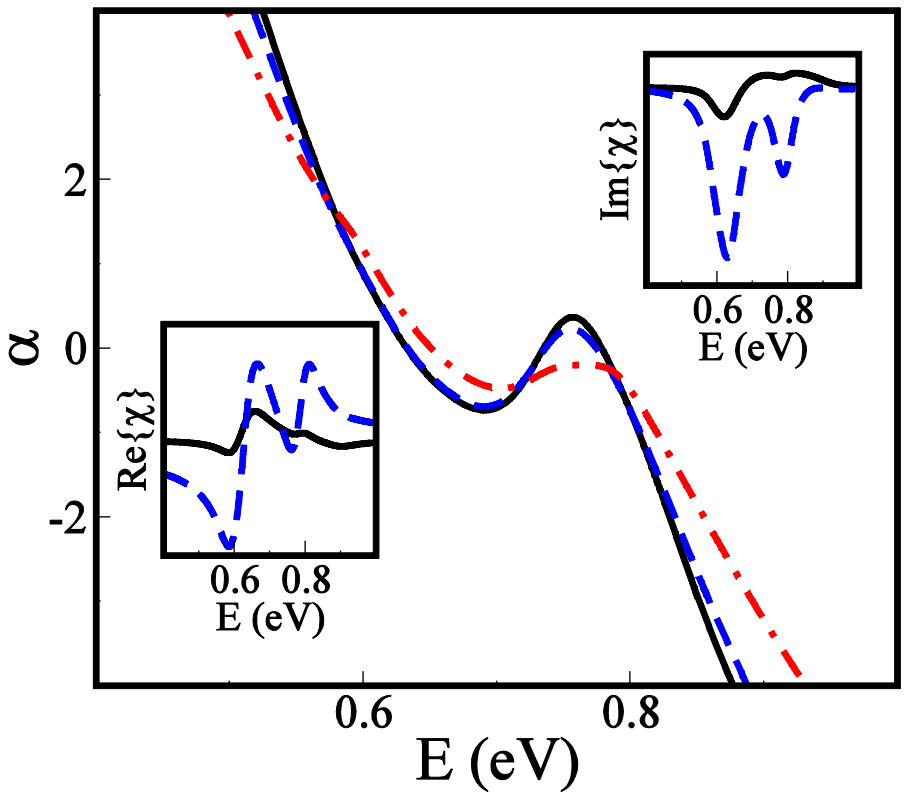

FIG. 1. Linewidth enhancement (α) factor for the 7 nm $Ga_{0.98}N_{0.02}As$-$Al_{0.3}Ga_{0.7}As$ quantum well of Ref. [11]. The solid-black, dashed-blue and dot-dashed-red curves have subband occupations given respectively by (N_{low}, N_{up}) = (1,1), (1,4) and (1,30) × 10^{11} cm^{-2}. The insets show corresponding real Re{χ} (left) and imaginary Im{χ} (right) parts of the susceptibility for the first two cases with matching color and curve codes.

Figure 2 compares the α factor spectrum at GWI with N_{low} = N_{up} considering both transitions (solid-black), e_3 to e_2 only (dashed-blue) and e_3 to e_1 only (dot-dashed-red). The insets depict real and imaginary parts of the optical susceptibility. Figure 3 puts the previous results in more complete perspective by depicting the value of α at peak gain as a function of carrier density.

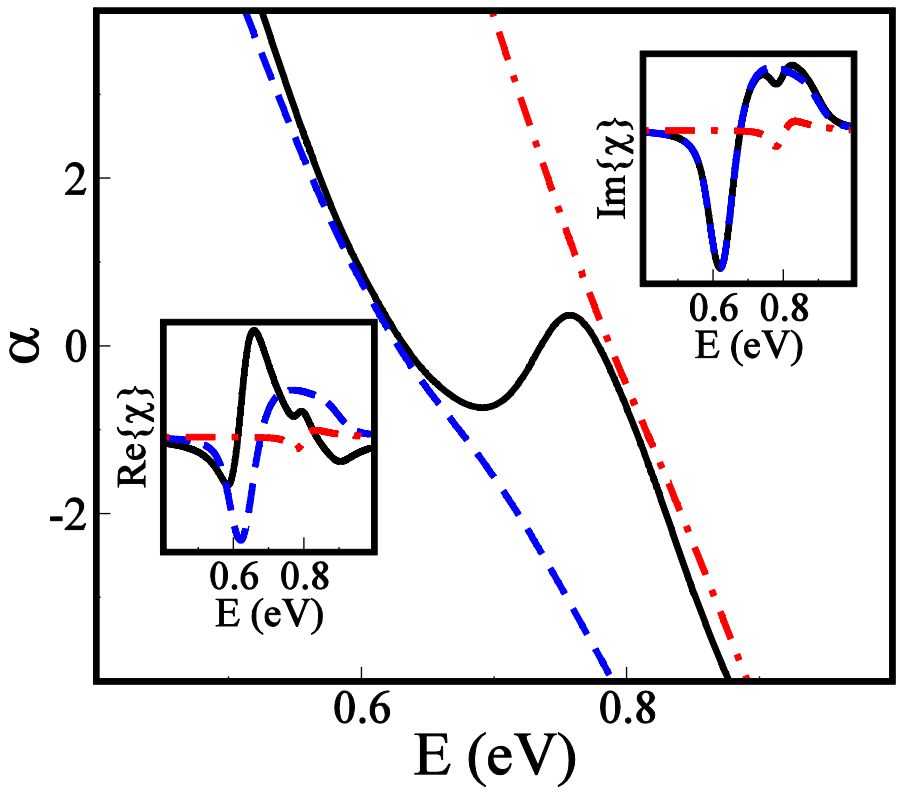

FIG.2. Linewidth enhancement (α) factor for the same sample in Fig.1. In all curves the subband occupations are $(N_{low},N_{up})= (1,1) \times 10^{11}$ cm^{-2}. The solid-black, dashed-blue and dot-dashed-red are respectively for both transitions, e_3 to e_2 and e_3 to e_1. The insets show corresponding real Re{χ} (left) and imaginary Im{χ} (right) parts of the susceptibility for the first two cases with matching color and curve codes.

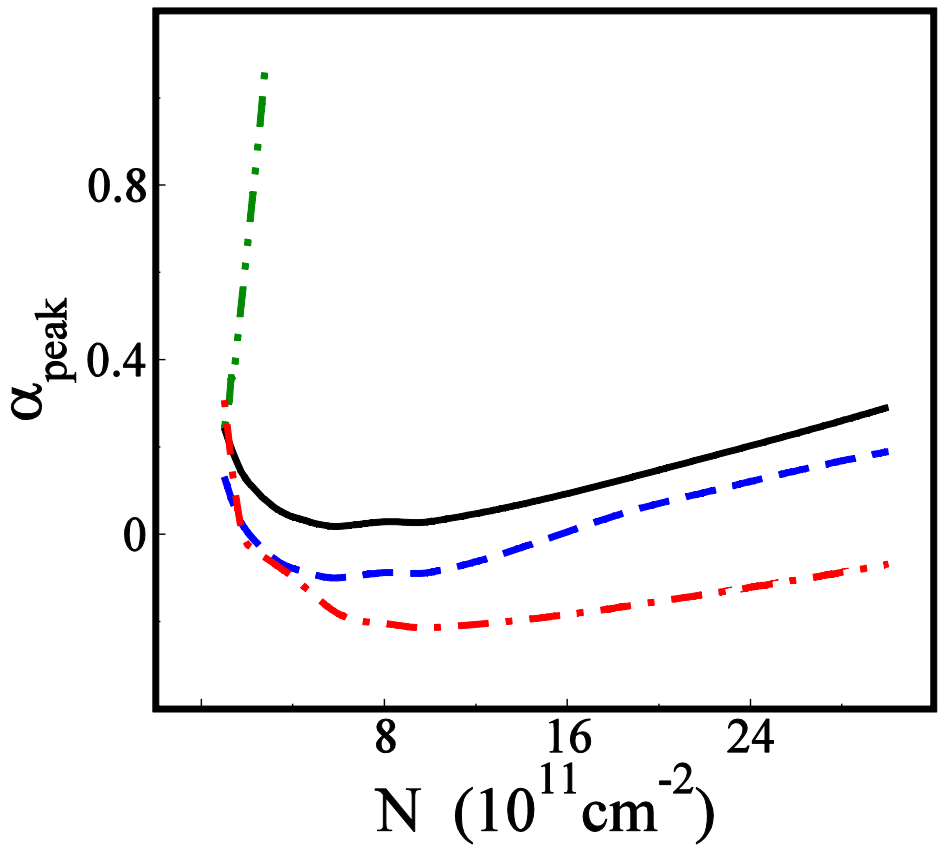

FIG.3. Linewidth enhancement (α) factor at peak gain for the same sample in Figs.1 and 2. The green dash-double-dotted curve has the upper subband e_3 occupation fixed at $N_{up} = 1 \times 10^{11}$ cm^{-2}, while the occupation of lower subbands N = N_{low} increase along the x-axis. The solid-black, blue-dashed and red dot-dashed curves have fixed occupation of the lower subbands e_1 and e_2 , $N_{low} = 1\times 10^{11}$ cm^{-2}, while the upper e_3 = subband occupation N = N_{up} increases along the x-axis. They are calculated, respectively, with both transitions included, only the e_3 to e_2 and only e_3 to e_1 transition considered.

The double peak feature in Im{χ} (and thus in the gain spectrum) in Figs. 1 and 2 due to the two transitions adds extra complexity to the α factor spectrum, leading to an "s-shaped" feature between 0.6 and 0.8 eV, which increases α at peak gain (solid black curve) compared to the cases where only one transition is taken into account (blue-dashed and red dot-dashed curves in Figs. 2 and 3).

When the occupations of lower subbands e_{3-} and e_{1-} are kept constant and the upper subband e_{2+} occupation is increased, there is an interplay of opposing effects. The upper band filling leads to a blue shift of the peak gain initially decreasing α at peak gain as it moves down in a relatively unchanged α spectrum, until the s-shape starts to be distorted due to a larger shape change in Re{χ} with respect to Im{χ}. See also the dot-dashed yellow curve in Fig.1. For the single transition case, which corresponds to the usual QCL inverted medium QCL case, even though the general qualitative behaviour is the same, without the "bump up" provided by the "s-shape", α at peak gain even reaches negative values. Both

negative and positive values as well as the evolution of α with injection current (and thus with carrier density) are consistent with experimental findings [6], even more so if the measurements cross from below to above threshold as in self-mixing experiments [5]. Different lasers will operate at different current injection and gain conditions, thus controlling the carrier distribution and peak gain position, determines at which value of α the laser will operate above threshold.

The scenario is different under gain without population inversion (green dash-double-dotted curve in Fig.3). The gain disappears fast with a larger number of global carriers in the lower bands. As the lower bands filling increases with the respect to the fixed density of the upper subband, the peak gain is red-shifted. Since the range within which GWI can be sustained is relatively small, the α factor spectrum remains essentially unaltered. Thus the value of α at peak gain increases fast due to the steep increase in the lower energy side of the spectrum.

Before wrapping up the results obtained, one very important point should be noted. Resonant tunneling plays an important role in the α factor, as demonstrated with a density matrix model employing the rotating wave approximation in Ref. [12]. Simulations for concrete QCL structures where resonant tunneling is included without the rotating wave approximation will be the target of forthcoming research.

In summary, this papers resolves the controversy created by intersubband α factors being measured with values ranging from -0.5 to 3, while they were expected to be zero. Counter rotating terms which are usually ignored because normally they do not affect the gain spectrum, are ultimately responsible for nonzero α at peak gain even without inclusion of nonparabolicity and manybody effects. These are however crucial to explain negative values. For laser without inversion conditions, where the gain spectrum is typically dispersive instead of Lorentzian, the α factor at peak gain is a bit larger, but still within the range of values found for conventional intersubband lasers. The dilute nitride quantum well structure chosen allows to control the gain lineshape of intersubband transitions from the usual Lorentzian to a dispersive shape for gain without inversion conditions and all numerical results are firmly within the range found experimentally, regardless of the fact that the photon energies are larger due to the selected transitions being not the usual two first conduction subbands, further highlighting the generality of the results. The results presented here have strong potential to further stimulate the development of practical lasing without inversion devices where more efficient room temperature

operation can be achieved and still with the same level of linewidth required for detailed spectroscopic applications.

ACKNOWLEDGMENTS

The author acknowledges support from MPNS COST ACTION MP1204 - TERA-MIR Radiation: Materials, Generation, Detection and Applications.

REFERENCES

[1]F. K. Tittel, D. Richter, and A. Fried, Topics Appl. Phys. 89, 445 (2003).

[2]A. L. Schawlow and C. H. Townes, Phys. Rev. 112 (6), 1940 (1958).

[3]C. H. Henry, IEEE J. Quantum Electron. 18 (2), 259 (1982).

[4]M. Lerttamrab, S.L. Chung, C. Gmachl, D.L Sivco, F. Capasso and A.Y. Cho, J. Appl. Phys. 94, 5426 (2003).

[5]J. von Staden,T. Gensty, M. Peil, W. Elsaesser, G. Giuliani, and C. Mann, Opt.Lett. 31, 2574 (2006).

[6]L. Jumpertz, F. Michel, R. Pawlus, W. Elsasser, K. Schires, M. Carras, and F. Grillot, AIP ADVANCES 6, 015212 (2016).

[7]R. P. Green, J.-H. Xu, L. Mahler, A. Tredicucci, F. Beltram, G. Giuliani, H. E. Beere, and D. A. Ritchie, Appl. Phys. Lett. 92, 071106 (2008).

[8]S. Fathololoumi, E. Dupont, C.W.I. Chan, Z.R. Wasilewski, S.R. Laframboise, D. Ban, A. Mátyás, C. Jirauschek, Q. Hu, and H. C. Liu, Opt. Express 20, 3866 (2012).

[9]A. Wacker, Nat. Phys. 3, 298 (2007).

[10]T. Schmielau and M.F. Pereira, Appl. Phys. Lett. 95, 231111 (2009).

[11]M.F. Pereira Jr. and S. Tomić, Appl. Phys. Lett. 98, 061101 (2011).

[12]T. Liu, K. E. Lee, and Q. J. Wang, Opt. Express 21, 27804-27815 (2013).

[13]M.F. Pereira Jr. and K. Henneberger, Phys. Rev. B58, 2064 (1998).

[14]M.F. Pereira Jr. and H. Wenzel, Phys. Rev. B 70, 205331 (2004).

[15]M.F. Pereira Jr., S.-C. Lee, and A. Wacker, Phys. Rev. B69, 205310 (2004).

[16]P. N. Hai, W. M. Chen, I. A. Buyanova, H. P. Xin, and C. W. Tu, Appl. Phys. Lett. 77, 1843 (2000).

[17]M.S. Vitiello, R.C. Iotti, F. Rossi, L. Mahler, A. Tredicucci, H.E. Beere, D.A. Ritchie, Q. Hu and G. Scamarcio, Appl. Phys. Lett. 100, 091101 (2012).